Differential pulse voltammetric determination of dopamine using Pd nanoparticles deposited on (3-aminopropyl)triethoxysilane functionalized CeO$_2$ nanoparticles

Muhammet GÜLER[*]
Department of Chemistry, Faculty of Science, Van Yüzüncü Yıl University, Van, Turkey

Abstract: In this study, a novel and effective electrochemical sensor for determination of dopamine (DA) was successfully developed by the modification of a glassy carbon electrode (GCE) using Pd nanoparticles deposited on (3-aminopropyl)triethoxysilane functionalized nanoceria (Pd@CeO$_2$-APTES) and nafion used as a protective membrane. The synthesized nanocomposites were evaluated using X-ray diffraction, high-resolution transmission electron microscopy, and Fourier transform infrared spectroscopy. Moreover, the electrochemical properties of the modified electrodes were investigated using cyclic voltammetry, electrochemical impedance voltammetry, and differential pulse voltammetry (DPV). The Nf/Pd@CeO$_2$-APTES/GCE showed a linear range of 2.5–149.5 μM for DA by DPV with a notable sensitivity of 0.83 mA mM^{-1} cm^{-2} and a low limit of detection of 0.46 μM based on the signal-to-noise ratio of 3 (S/N = 3). In addition, the sensor exhibited satisfactory selectivity, remarkable sensitivity, repeatability, and reproducibility. The sensor protected 92.07% of its initial electrocatalytic activity toward the oxidation of dopamine after 30 days. The Nf/Pd@CeO$_2$-APTES/GCE was used for determination of DA in serum samples. The results indicate that the sensor can be a notable device for the detection of DA in biological fluids.

Key words: Pd nanoparticles, (3-aminopropyl)triethoxysilane, nanoceria, differential pulse voltammetry, dopamine

1. Introduction

Dopamine (DA), a catecholamine substance and catalyzed by monoamine oxidase and catechol-O-methyltransferase enzymes, is widely found in the mammalian brain and central nervous system and has an important role in the function of memory and learning.[1,2] DA has attracted a great deal of attention in medical research owing to the fact that it plays a vital role in motor and cognitive functions. Determination of DA is very important for diagnosing, tracking, and treating neurological failures such as Alzheimer's, Parkinson's, and schizophrenia, which is ascribed to abnormal levels of DA in the brain.[3] Thus, high concentrations of DA in biological fluids (serum, urine) are a very important pathological marker.

To date, various methods, such as high-performance liquid chromatography,[4] electrochemical sensors,[5−7] fluorometry,[8] colorimetry,[9] electrochemiluminescence,[10] and flow injection analysis,[11] have been performed to determine DA in biological fluids. However, these methods include high-cost equipment and complicated systems, and are time-consuming compared to electrochemical sensors and biosensors. Electrochemical methods have been frequently used for the determination of DA because they are easy to prepare, very sensitive and selective, and comparatively low-cost. However, it is difficult to detect dopamine electrochemically because it

---

[*]Correspondence: mguler@yyu.edu.tr

oxidizes at nearly the same potential as some electroactive species such as ascorbic acid (AA) and uric acid (UA), which can cause the overlapping of the voltammetric peak responses to the oxidation of DA.[12] For this reason, it is essential to develop a selective, sensitive, rapid, and simple method for the electrochemical determination of DA in the presence of electroactive species.

In recent years, nanocomposites based on metal nanoparticles have been commonly used for the electrochemical detection of DA, UA, AA, hydrogen peroxide, glucose (Glu), and other electroactive species because metal nanocomposites are easy to prepare and have electrochemical stability, good electrocatalytic behavior, and biocompatibility. For example, polythionine/AuNPs modified glassy carbon was used for the determination of DA. The sensor detected DA in the linear range of 7.5–320 nM. Also, the detection limit was 2.8 nM.[13] In another study, two-dimensional Pd nanoparticles were generated for DA determination. The linear range for DA was between 0.05 and 130 μM with a detection limit of 25 nM.[14] Wang et al. reported UA and DA sensor based on the modified glassy carbon electrode (GCE) using cubic Pd deposited on reduced graphene oxide. The working electrode exhibited a linear range of 0.45–421 μM with a detection limit of 0.18 μM for DA and 6–469.5 μM with a detection limit of 1.6 μM for uric acid.[15] Guler et al. used (3-aminopropyl)triethoxysilane (APTES) functionalized reduced graphene oxide and Pd@Ag bimetallic nanoparticles deposited on reduced graphene oxide for the determination of hydrogen peroxide and Glu.[16,17]

As one of the most commonly used rare metal oxides in the world, cerium dioxide (ceria, CeO_2) has been used in many applications such as corrosion prevention, solid-state electrolytes for fuel cells, oxygen sensors, catalysts for automotive exhaust treatment, wear-resistant coatings, and luminescence materials because of its unusual oxygen storage capacities, excellent ionic conductivity, good optical properties, remarkable catalytic properties, and relatively low cost.[18−21]

To the best of our knowledge, Nf/Pd@CeO_2-APTES nanocomposites have not yet been studied for the electrochemical determination of DA in the presence of AA, UA, folic acid (FA), and Glu. In the present study, we proposed sensitive, selective, rapid, and low-cost synthesis of Pd nanoparticles loaded on APTES-functionalized CeO_2 for the detection of DA in the presence of some electroactive species such as AA and UA. Nafion (Nf) was used as a protective membrane for the composite.[16,17,22] The structure of the nanocomposites was characterized by means of X-ray powder diffractometer (XRD), Fourier transform infrared spectroscopy (FTIR), and transmission electron microscopy (TEM). Moreover, the electrochemical behavior of the Nf/Pd@CeO_2-APTES nanocomposites was investigated using cyclic voltammetry (CV), electrochemical impedance spectroscopy (EIS), and differential pulse voltammetry (DPV). The fabricated sensor based on Nf/Pd@CeO_2-APTES displayed very good electrocatalytic ability for the determination of DA and a notable linear range, low limit of detection, and satisfactory sensitivity and selectivity when compared with the studies reported previously.

2. Results and discussion
2.1. Characterization of CeO_2-APTES and Pd@CeO_2-APTES nanocomposites

In order to evaluate the surface modification of CeO_2, FTIR was performed. The FTIR spectra of CeO_2-OH and CeO_2-APTES are depicted in Figure 1. In the spectrum of the hydroxylated CeO_2 (Figure 1a), the broad band at 3470 cm^{-1} can be attributed to the –OH band. As can be seen in Figure 1b, the chemical interactions between CeO_2-OH and APTES created some clear bands at 1122, 1130, 1334, 1635, 2935, and 3441 cm^{-1}, corresponding to Si–O–C, Si–O–Si asymmetric stretching, Si–C, Ce–O, CH_2, and –NH_2 bands, respectively, demonstrating strong interactions between the support and APTES.

As seen in Figure 2, the crystal structure of CeO_2-APTES (Figure 2a) and Pd@CeO_2-APTES (Figure 2b) nanocomposites was evaluated using XRD. The diffraction peaks at 28.5°, 33°, 47.5°, 56.5°, and 59° are ascribed to (111), (200), (220), (311), and (222), respectively, corresponding to the crystal planes of CeO_2 (JPDS = 43–1002). The presence of Pd nanoparticles is clearly seen in Figure 2b along with the diffraction peaks of nanoceria. That is to say, the peak at 40.2° is attributed to the crystal plane of (111) face-centered cubic (Fcc) Pd nanoparticles.
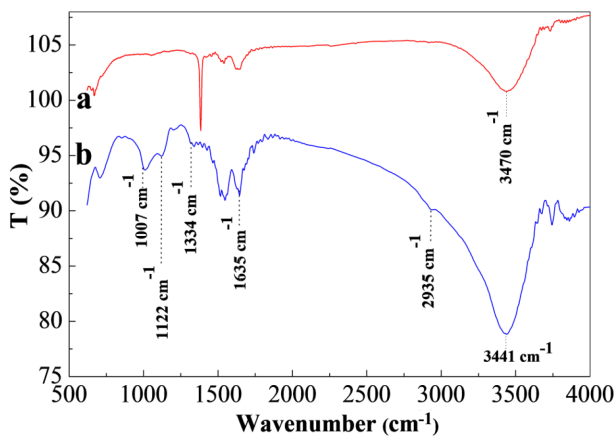

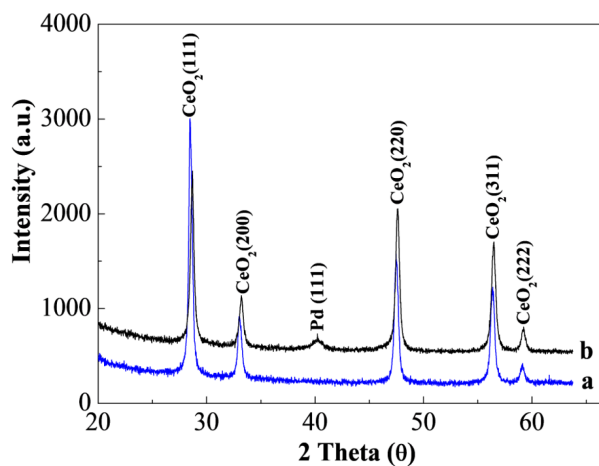**Figure 1**. FTIR spectra (a) CeO_2-OH and (b) CeO_2-APTES.

Figure 2. XRD patterns of (a) CeO_2-APTES and (b) Pd@CeO_2-APTES.

The surface morphology of nanoceria (Figure 3A) and the size of Pd nanoparticles (Figure 3B) were investigated by means of high-resolution TEM, which demonstrates that Pd nanoparticles 0.82–2.0 nm in size were uniformly anchored on CeO_2 nanoparticles.
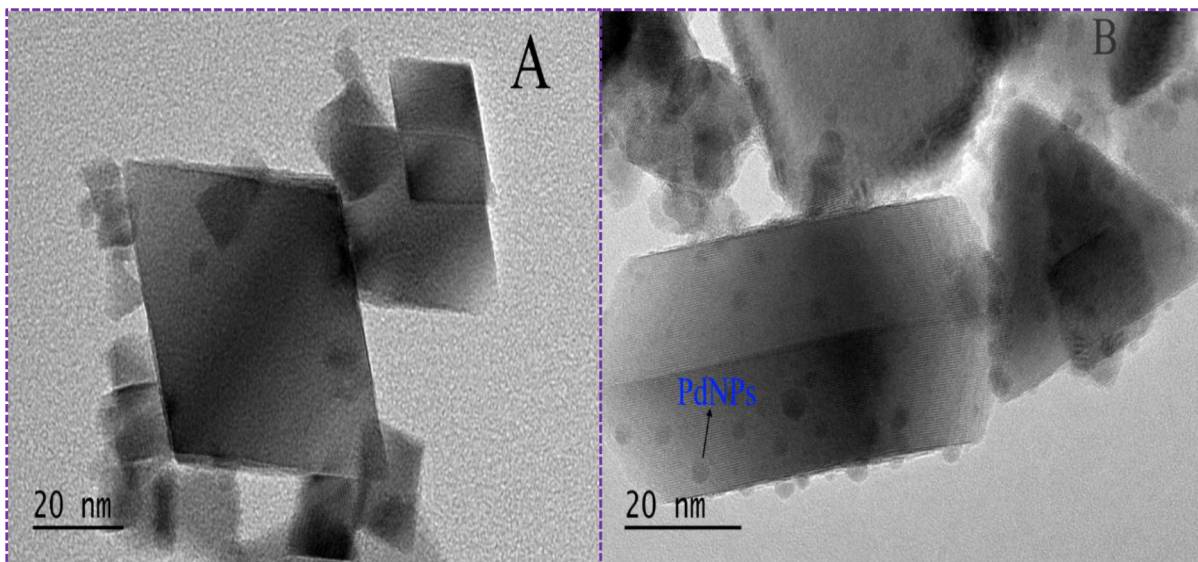

Figure 3. TEM images of CeO_2-APTES (A) and Pd@CeO_2-APTES (B).

2.2. Electrochemical behaviors of CeO$_2$-APTES and Pd@CeO$_2$-APTES nanocomposites

EIS is an effective method for evaluating the electron transfer process occurring on the electroactive surface area of modified working electrodes. In a typical Nyquist graph, there is a linear part and a semicircular part. The linear part at the low frequencies explains the diffusion process and the semicircular part at the high frequencies accounts for the electron transfer kinetics on the working electrode. The diameter of the semicircular part is equal to the electron transfer resistance (R_{ct}).[23] In this study, the EIS of bare GCE, Nf/CeO$_2$-APTES/GCE, and Nf/Pd@CeO$_2$-APTES/GCE was performed in 5.0 mM K$_3$Fe(CN)$_6$/K$_4$Fe(CN)$_4$ (1:1) including 0.1 M KCl (Figure 4). The R_{ct} values of GCE (Figure 4a), Nf/CeO$_2$-APTES/GCE (Figure 4b), and Nf/Pd@CeO$_2$-APTES/GCE (Figure 4c) were 5, 52, and 28 kΩ, respectively. The semicircular diameter of CeO$_2$-APTES decreased after anchoring Pd nanoparticles on it, demonstrating the successful fabrication of Pd@CeO$_2$-APTES. Furthermore, the presence of Nf used as a protective membrane causes the increase in electron transfer resistance.
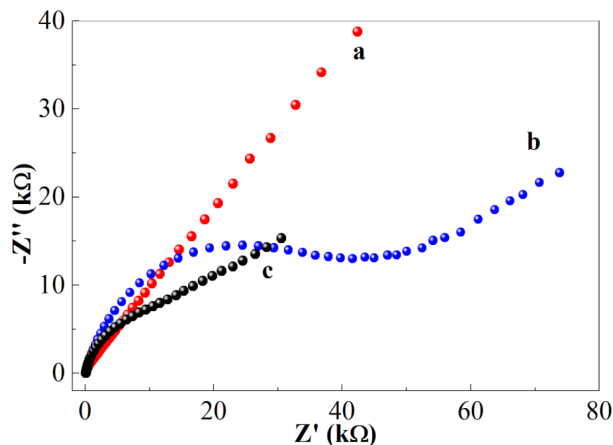

Figure 4. Electrochemical impedance Nyquist plot of bare GCE (a), Nf/CeO$_2$-APTES/GCE (b), and Nf/Pd@CeO$_2$-APTES/GCE (c) in 5 mM [Fe(CN)$_6$]$^{3-/4-}$ (1:1) and 0.1 M KCl. Frequency range: 0.01 Hz to 100 kHz; applied potential: 0.2 V.

The electrochemical behavior of DA in the bare GCE, Nf/CeO$_2$-APTES/GCE, and Nf/Pd@CeO$_2$-APTES/GCE was investigated using CV in 0.1 M phosphate buffer solution (PBS, pH 7) in the absence and presence of DA. Figure 5 displays the cyclic voltammograms of the bare GCE (Figure 5a), Nf/CeO$_2$-APTES/GCE (Figure 5b), and Nf/Pd@CeO$_2$-APTES/GCE (Figure 5c) in the absence of DA in the potential range of –0.2 to 0.8 V. When 0.1 mM of DA was put into the electrochemical cell, a very poor oxidation peak of DA was observed at the bare GCE (Figure 5a′). However, the oxidation peak of DA at the Nf/CeO$_2$-APTES/GCE was better than that at the GCE (Figure 5b′). After modification using Nf/Pd@CeO$_2$-APTES, the working electrode exhibited the best oxidation peak of DA at 0.2 V and a scan rate of 0.05 V/s (Figure 5c′), indicating that small Pd nanoparticles increased the electron transfer of DA on the working electrode. The oxidation peak current of DA at Nf/Pd@CeO$_2$-APTES/GCE was 9.72 times higher than the one observed with the bare GCE.

2.3. Effect of pH and scan rate

The influence of pH on the Nf/Pd@CeO$_2$-APTES/GCE response to 40 μM DA was investigated using DPV. As seen in Figure 6, when pH increased from 5 to 8.5, the oxidation potential of DA decreased, demonstrating that the proton took part in the electrochemical reaction of DA. The regression equation obtained here for E_{pa} versus pH can be represented as follows:
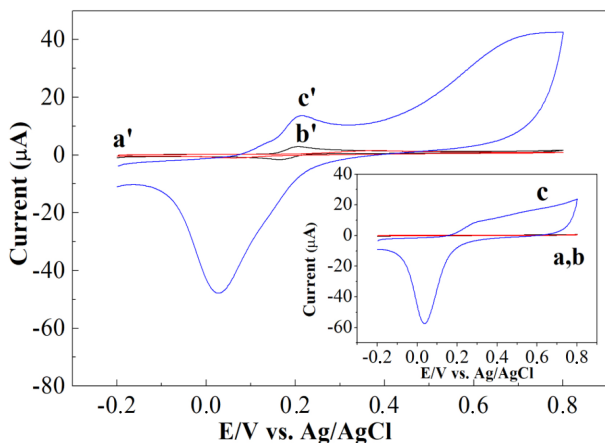

Figure 5. CVs of bare GCE (a), Nf/CeO$_2$-APTES/GCE (b), and Nf/Pd@CeO$_2$-APTES/GCE (c) in the absence of DA and bare GCE (a$'$), Nf/CeO$_2$-APTES/GCE (b$'$), and Nf/Pd@CeO$_2$-APTES/GCE (c$'$) in 0.1 M PBS (pH 7) containing of 0.1 mM of DA at a scan rate of 0.05 V/s.
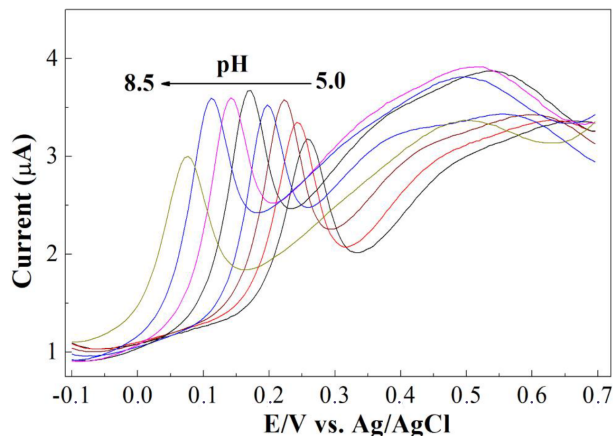
Figure 6. DPVs of Nf/Pd@CeO$_2$-APTES/GCE in 0.1 mM PBS with various pH (from 5.0 to 8.5) containing 40 μM DA.

$$E_{pa} = -0.0517pH + 0.5284(R^2 = 0.9958) \tag{1}$$

According to the equation, the obtained slope was –51.7 mV/pH (Figure 7a), which complies with the theoretical value of –59 mV/pH. The results indicate that the number of protons and electrons exchanged in the process is equal.[24] Moreover, the maximum current was observed at a pH value of 7.0 (Figure 7b). Thus, pH 7 was used for further experiments.

The electroactive surface area of bare GCE (Figure 8a), Nf/CeO$_2$-APTES/GCE Figure 8b), and Nf/Pd@CeO$_2$-APTES/GCE (Figure 8c) was determined using CVs in 5 mM [Fe(CN)$_6$]$^{3-/4-}$ solution including 0.1 M KCl. The peak current (I_p) is proportional to the square root of the scan rate ($\nu^{1/2}$) as depicted in the following Randles–Sevcik equation:

$$I_p = (2.69 \times 10^5)n^{3/2}AD_0^{1/2}C_0 \tag{2}$$

Here n is the number of electrons participating in the electrochemical reaction, A is the active surface area of the working electrode (cm^2), D_o is the diffusion coefficient (cm^2 s^{-1}), I_p is the peak current (A), C_o is the concentration of the electroactive species (mol L^{-1}), and is the scan rate (V s^{-1}).[25] D_o, as determined by Konopka and McDuffie, is 6.56×10^{-6} cm^2 s^{-1} at 25 °C for 5 mM of K$_3$Fe(CN)$_6$/K$_4$Fe(CN)$_4$ (1:1) containing 0.1 M KCl.[26] For this, CVs were obtained using the bare GCE, Nf/CeO$_2$-APTES/GCE, and Nf/Pd@CeO$_2$-APTES/GCE at various scan rates (0.04 to 0.26 V s^{-1}). After that, the electrochemically active surface area was calculated to be 0.089 cm^2 for the bare GCE, 0.01 cm^2 for Nf/CeO$_2$-APTES/GCE, and 0.056 cm^2
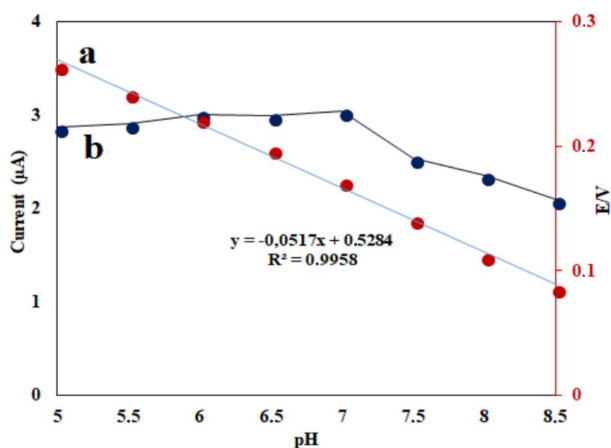
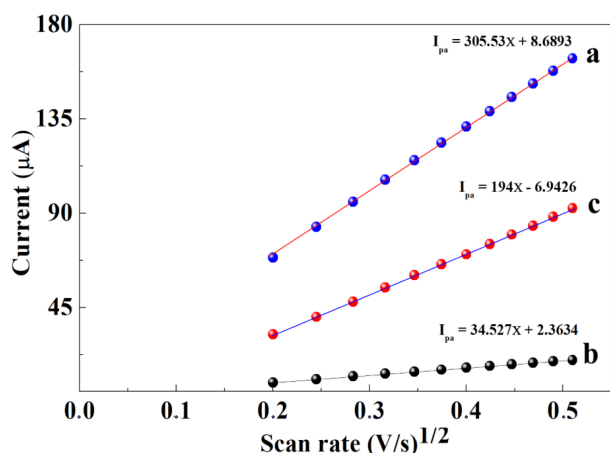**Figure 7**. Plot of peak potential (a) and oxidation peak current (b) of 40 μM DA against pH in 0.1 M PBS.

Figure 8. Plot of oxidation peak current of 5 mM $[Fe(CN)_6]^{3-/4-}$ (1:1) at bare GCE (a), CeO_2-APTES (b), and Nf/Pd@CeO_2-APTES/GCE (c) versus square root of scan rate (scan rate: 0.02–0.26 V/s).

for Nf/Pd@CeO_2-APTES/GCE by using the slope of I_p versus $\nu^{1/2}$ graph, indicating that Pd nanoparticles increased the active surface area of the working electrode. Furthermore, the ratio of the anodic and cathodic peak current was 1.03 (approximately 1.0), which demonstrated a typical reversible electrode process taking place at the Nf/Pd@CeO_2-APTES/GCE electrode.

In order to detect charge transfer coefficient (α), the number of electrons involved in the electrochemical reaction (n), and electron transfer rate constant (k_s), the following equations were used:[27]

$$E_{pa} = E^0 + \frac{2.303RT}{(1-\alpha)nF} \log \nu \tag{3}$$

$$E_{pc} = E^0 + \frac{2.303RT}{\alpha nF} \log \nu \tag{4}$$

$$\log k_s = \alpha \log(1-\alpha) + (1-\alpha)\log \alpha - \frac{\log RT}{nF\nu} - \frac{\alpha(1-\alpha)nF\Delta E}{2.303RT} \tag{5}$$

Figure 9 shows CVs of 0.5 mM DA at different scan rates. The plot of anodic and cathodic peak current versus the scan rate was linear when the scan rate increased from 20 to 260 mV/s, which proves that the electrochemical oxidation of DA on the Nf/Pd@CeO_2-APTES/GCE sensor is an adsorption-controlled process. The anodic and cathodic peak potential separation increased with increasing scan rate, demonstrating limitation because of charge transfer kinetics. So as to calculate α, n, and k_s, the linear regression equation of anodic and cathodic peak potential of DA against lnn were obtained (Figures 10a and 10b and Eqs. (6), (7)).

$$E_{pc} = -0.0219 \ln \nu + 0.0669 \tag{6}$$

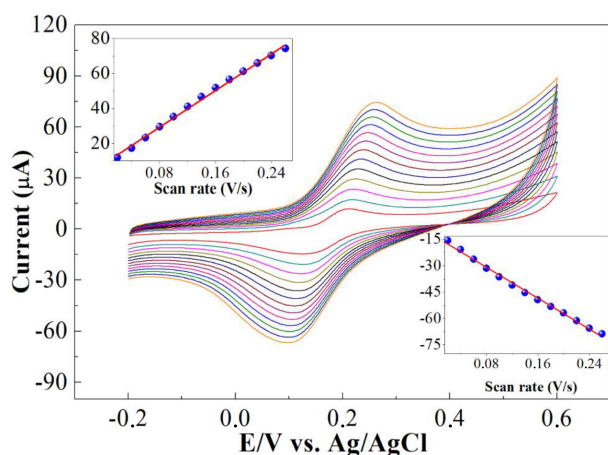$$E_{pa} = 0.0359 \ln \nu + 0.3102 \tag{7}$$

Figure 9. CVs response of Nf/Pd@CeO$_2$-APTES/GCE to 0.1 mM of DA in 0.1 PBS (pH 7) at different scan rates (from 0.02 to 0.26 V/s). Insets: the plot of oxidation and reduction of DA versus scan rate (V/s).
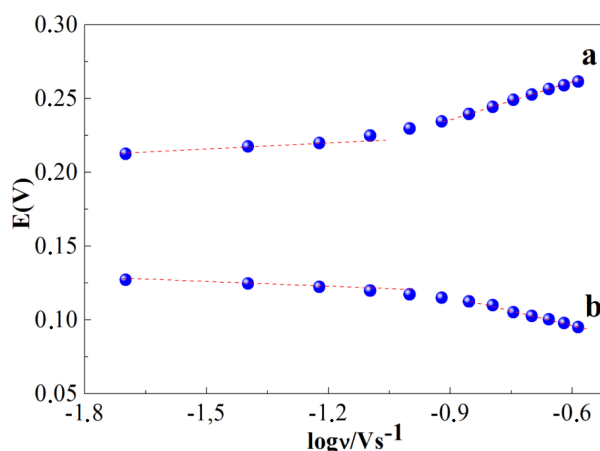
Figure 10. Plot of oxidation and reduction peak potential (V) versus log n for Nf/Pd@CeO2-APTES/GCE.

From the slope and intercept of these equations, α, n, and k_s were calculated to be 0.62, 1.89, and 0.59 s^{-1}, respectively. The electron transfer rate constant obtained in this study was smaller than those in previous reports (Table 1). It is because Nf decreased the electron transfer rate on the working electrode.

Table 1. Comparison of DPVs response of Nf/Pd@CeO$_2$-APTES/GCE to DA with the studies previously reported.

Electrode	Sensitivity (μA/μM)	Linear range (μM)	LOD (μM)	k_s (s^{-1})	Ref.
pHQ/AuNPs/Nf	6.663	0.1–10	0.04	-	5
$\alpha-$WO$_3$/GCE	-	0.1–50, 50–600	0.024	1.121	12
PTh/AuNPs	-	0.0075–0.32	0.0028	-	13
PdNP/ITO	0.17	5.0–130	0.025	-	14
PdNP/CNF/CPE	-	0.5–160	0.2	-	28
Au-Cu$_2$O/rGO	-	10–90	3.9	1.56	29
ZrO$_2$-GRP-CHIT	22	1–5	0.0113	-	30
3DGH-Fc/GCE	-	10–180	0.042	-	31
Au/P-G hybrid	-	0.1–180	0.002	-	33
3D N, P-doped carbon	-	2–200	0.6	-	34
Graphene-MoS$_2$/GCE	-	0.05–10	0.00713	-	35
PdNP/PMPy/Pt	0.0056, 0.71	0.1–10	0.012	-	36
PdNP/GCE	0.31	8-88	-	-	37
AuNP/Pd	0.015	0.5-1000	0.08	-	38
PdNP/GR/CS/GCE	0.32	0.5–15, 20–200	0.1	-	39
RGO/PdNP/GCE	0.21	1.0–150	0.233	-	40
PdNP/CNF/CPE	-	0.5–160	0.2	-	41
Nf/Pd@CeO$_2$-APTES/GCE	0.0467	2.5–149.5	0.46	0.59	This work

2.4. Performance of Nf/Pd@CeO$_2$-APTES/GCE sensor for DA determination

After the optimum conditions for the electrochemical determination of DA at the Nf/Pd@CeO$_2$-APTES/GCE sensor were detected, the oxidation current against voltage (versus Ag/AgCl) was obtained in 0.1 M PBS (pH 7) (Figure 11). The linear detection range for DA concentration was detected upon addition of DA to PBS. To ensure that DA was homogeneously mixed in the solution, the electrolyte was stirred for about 30 s. The maximal current response of the sensor to the oxidation of DA was obtained at 0.167 V. The oxidation peak current was proportional to the concentration of DA with a linear range of 2.5–149.5 μM and the linear equation of I_{pa} (μA) = 0.0467 DA (μM) + 1.6577 (R^2 = 0.9976). In addition, the sensor showed a notable sensitivity of 0.83 mA mM^{-1} cm^{-2} and a low limit of detection (LOD) of 0.46 μM according to signal-to-noise ratio of 3 (S/N = 3). The results achieved in this study using the Nf/Pd@CeO$_2$-APTES/GCE sensor were compared with other DA determination sensors reported in different literature (Table 1), which demonstrates that the fabricated sensor exhibited satisfactory electrocatalytic response to the oxidation of DA due to the specific surface area, high conductivity, and biocompatibility of the nanocomposite.

2.5. Selectivity, reproducibility, and storage stability of Nf/Pd@CeO$_2$-APTES/GCE

In order to study the selectivity of Nf/Pd@CeO$_2$-APTES/GCE sensor, the interfering effect of AA, UA, Glu, and FA coexisting compounds in biological fluids on the sensor response was investigated. Figure 12 shows the DPVs of different concentrations of DA (from 40 to 130 μM) in the presence of AA, UA, Glu, and FA (from 40 to 130 μM). As seen in the figure, no important DPV responses were detected in the presence of the interferences except that an oxidation peak was observed at 0.34 V belonging to the oxidation of 0.13 mM UA. However, the oxidation of UA did not affect the response of the sensor to DA, demonstrating the good selectivity of Nf/Pd@CeO$_2$-APTES/GCE toward DA. In addition, no electrocatalytic response for AA, FA, or Glu was observed. The reason for this could be that AA was negatively charged (pKa = 4.10) at pH 7.0, whereas DA was positively charged (pKa = 8.87) at this pH.
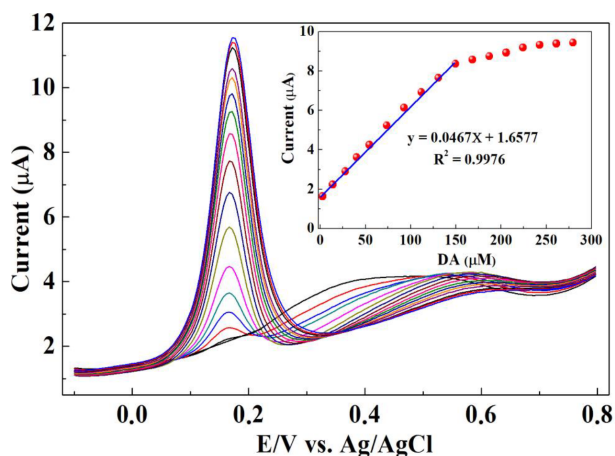

Figure 11. DPVs obtained at Nf/Pd@CeO2-APTES/GCE working electrode with various concentrations of DA. Inset: oxidation peak current of DA versus concentration of DA.
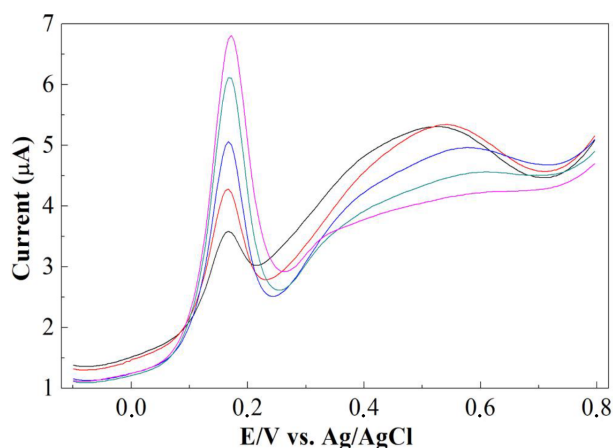
Figure 12. Interference study. DPVs response of Nf/Pd@CeO$_2$-APTES/GCE to 40, 50, 70, 100, and 130 μM of DA in the presence of 40, 50, 70, 100, and 130 μM of AA, UA, Glu, and FA.

To investigate the repeatability of Nf/Pd@CeO$_2$-APTES/GCE working electrode, five different DPVs were obtained in 0.1 M PBS (pH 7) containing 40 μM DA using the same modified electrode. Relative standard deviation (RSD%) of these five successive measurements was 0.67, revealing an excellent repeatability for the sensor.

The reproducibility of the sensor was investigated using five independent Nf/Pd@CeO$_2$-APTES/GCE electrodes. The calculated RSD% was 2.03, which was in good agreement with those reported previously.[13,29,31]

The storage stability of the sensor was also evaluated by measuring the decrease in the oxidation current of 40 μM DA during repetitive DPV measurements for every week over 1 month. After 30 days, the sensor protected 92.07% of its initial current response to the oxidation of DA with a standard error of 0.83 (n = 6), indicating that Pd@CeO$_2$-APTES was a good electrochemical catalyst for the DA detection.[5,32]

2.6. Determination of DA in real samples

To evaluate the applicability of the Nf/Pd@CeO$_2$-APTES/GCE sensor and detect DA concentration in a serum sample, the serum sample was diluted 20 times using 0.1 M PBS (pH 7) before test. As depicted in Table 2, the RSD% was less than 3 and the recovery was between 100.16 and 102.28 according to the standard addition method, demonstrating that Nf/Pd@CeO$_2$-APTES/GCE showed good applicability for DA determination in serum samples.

Table 2. Detection of DA in serum samples using Nf/Pd@CeO$_2$-APTES/GCE working electrode (n = 5).

Serum	Added (μM)	Found (μM)	RSD (%)	Recovery (%)
1	-	not detected	-	-
2	10	10.22	2.55	102.20
3	50	51.08	1.98	100.16
4	80	80.95	1.74	101.19
5	120	122.74	2.97	102.28

2.7. Conclusion

In this study, a novel and effective DA sensor depending on Pd nanoparticles deposited on CeO$_2$-APTES was successfully prepared. APTES was used to synthesize relatively small Pd nanoparticles on nanoceria rather than sensing DA in biological fluids. The TEM image reveals that the desired aim was achieved and the nanoparticles were homogeneously dispersed on the support. Moreover, the nanocomposites were evaluated using FTIR, XRD, CV, EIS, and DPV. The sensor exhibited a linear range of 2.5–149.5 μM for the detection of DA using DPV with a correlation coefficient of 0.9976. The detection limit and sensitivity were 0.46 μM and 0.83 mA mM^{-1} cm^{-2}, respectively, which was in good agreement with previous DA studies. In addition, it is surprising that AA did not exhibit an oxidation peak at the prepared sensor, which is another advantage of the sensor for determination of DA. The sensor displayed good sensitivity, selectivity, repeatability, and reproducibility with respect to electrochemical oxidation of DA. Taking these results into account, the constructed sensor is a promising tool for future studies of the electrochemical determination of electroactive compounds.

3. Experimental

3.1. Chemicals and apparatus

Cerium oxide (CeO_2), DA, Nf solution (5% in a mixture of aliphatic alcohols and water), $PdCl_2$, KCl, AA, FA, UA, Glu, APTES, and toluene were purchased from Sigma-Aldrich (St. Louis, MO, USA). Before working electrode modification 0.125% of Nf solution was prepared using ethanol. Ethanol, methanol, and ammonia solutions and all other chemicals for electrochemical studies were purchased from Merck (Kenilworth, NJ, USA). A Metrohm Autolab PGSTAT128N Potentiostat was used for electrochemical measurements (Herisau, Switzerland). XRD (D8 Advance; Bruker, Billerica, MA, USA), high-resolution TEM, (JEM-2100; JEOL, Tokyo, Japan), and FTIR (Shimadzu, Kyoto, Japan) were used for the characterization of the nanocomposites. Glassy carbon working electrode (GCE), Ag/AgCl (3 M KCl) reference electrode, and platinum wire counter electrode were obtained from BASi Corporation (West Lafayette, IN, USA).
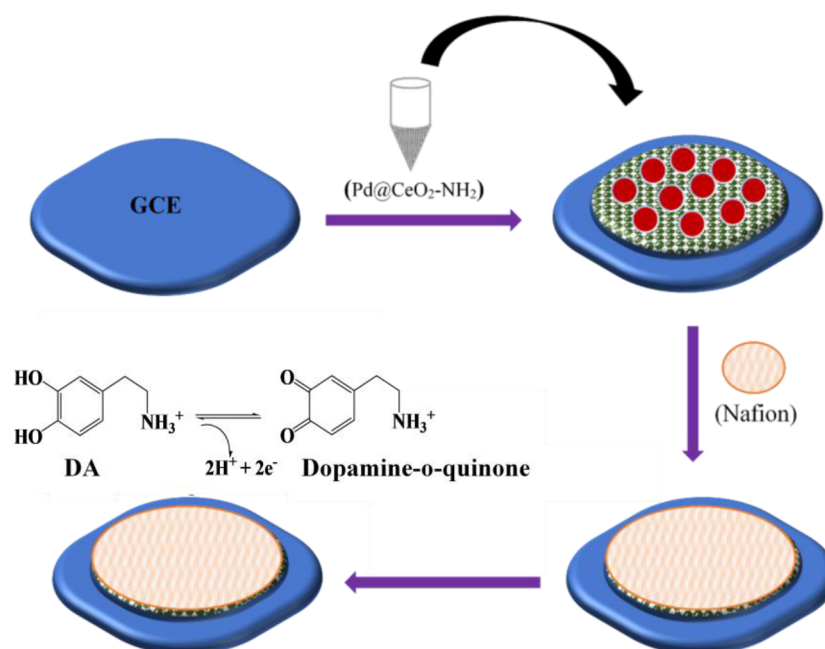
3.2. Preparation of Pd@CeO$_2$-APTES

For the synthesis of hydroxylated CeO_2 (CeO_2-OH), 0.5 g of CeO_2 was added to a round-bottom flask containing 25 mL of ethanol. Then 8 mL of the concentrated ammonia solution (30%) was rapidly added to the mixture and it was stirred for 12 h at laboratory temperature (about 25 °C). The resulting product was filtrated by means of filter paper and washed with twice-distilled water (3 × 20 mL) and ethanol (3 × 20 mL), respectively, and dried in a vacuum oven at 150 °C.

In order to prepare CeO_2-APTES, a desirable amount of APTES was added to 30 mL of dry toluene including 0.5 g of CeO_2-OH. The mixture was stirred for about 12 h. After that, the precipitate was filtrated and washed with toluene (3 × 20 mL). Lastly, the product was dried using a vacuum oven at 150 °C for 1 h.[42]

For preparation of Pd@CeO_2-APTES, 0.1 g of CeO_2-APTES was put into 5 mL of twice-distilled water including $PdCl_2$ (29.4 mg, 0.166 mmol). The mixture was stirred for 3 h to allow the interaction between the support and the nanoparticles. Then to reduce the composite, 1 mL of freshly prepared $NaBH_4$ (2.49 mmol, 94.2 mg) solution was put into the continuously stirred mixture at room temperature. It was stirred for some time in order to complete the reduction. The resulting product was filtered and washed with twice-distilled water (3 × 20 mL) and ethanol (3 × 20 mL), respectively. The achieved Pd@CeO_2-APTES nanocomposites were dried using a vacuum oven at 150 °C for 1 h.[43]

3.3. Preparation of Nf/CeO$_2$-APTES/GCE and Nf/Pd@CeO$_2$-APTES/GCE

Prior to modification, GCE was polished with alumina slurry and sonicated using HNO_3/H_2O (1:1), ethanol, and twice-distilled water for 5 min, respectively. Then 5 mg of Pd@CeO_2-APTES nanocomposites were put into 1 mL of ethanol and sonicated for 20 min with an ultrasonic cleaner. For the fabrication of Nf/Pd@CeO_2-APTES/GCE, 5 µL of this dispersion was loaded on the GCE by drop-casting and dried at room temperature. Later, 3 µL of Nf solution (0.125% in ethanol) was dropped on Pd@CeO_2-APTES/GCE and the modified electrode was allowed to dry under room temperature. The Nf/CeO_2-APTES/GCE sensor was constructed using the same procedure mentioned above for the fabrication of the Nf/Pd@CeO_2-APTES/GCE sensor.[44] The Scheme shows the schematic fabrication of the Nf/Pd@CeO_2-APTES/GCE sensor.

Scheme. Step-by-step fabrication of Nf/Pd@CeO$_2$-APTES/GCE working electrode.

3.4. Preparation of serum samples and DA determination

Practical application of the Nf/Pd@CeO$_2$-APTES/GCE sensor was evaluated in human serum samples obtained from Faculty of Medicine, Yüzüncü Yıl University, Van, Turkey. For this, the serum samples were centrifuged at 4000 rpm for 15 min. Then the supernatant was diluted 20 times with 0.1 M PBS (pH 7.0) and divided into five portions. The first portion was used for determination of DA in the serum. Then various concentrations of DA were added to the other portions. Lastly, DA was determined in the portions using DPV.

References

1. Robinson, D. L.; Venton, B. J.; Heien, M. L. A. V.; Wightman, R. M. *Clin. Chem.* **2003**, *49*, 1763-1773.

2. Hefco, V.; Yamada, K.; Hefco, A.; Hritcu, L.; Tiron, A.; Nabeshima, T.; *Eur. J. Pharmacol.* **2003**, *475*, 55-60.

3. Hyman, S. E.; Malenka, R. C. *Nat. Rev. Neurosci.* **2001**, *2*, 695-703.

4. De Benedetto, G. E.; Fico, D.; Pennetta, A.; Malitesta, C.; Nicolardi, G.; Lofrumento, D. D.; De Nuccio, F.; La Pesa, V. *J. Pharm. Biomed. Anal.* **2014**, *98*, 266-270.

5. Li, X.; Lu, X.; Kan, X. J. *Electroanal. Chem.* **2017**, *799*, 451-458.

6. Rithesh Raj, D.; Prasanth, S.; Vineeshkumar, T. V.; Sudarsanakumar, C. *Sens. Act. B Chem.* **2016**, *224*, 600-606.

7. Üğe, A.; Koyuncu Zeybek, D.; Zeybek, B. *J. Electroanal. Chem.* **2018**, *813*, 134-142.

8. Suzuki, Y. *Sens. Act. B Chem.* **2017**, *239*, 383-389.

9. Wen, D.; Liu, W.; Herrmann, A. K.; Haubold, D.; Holzschuh, M.; Simon, F.; Eychmüller, A. *Small* **2016**, *12*, 2439-2442.

10. Li, L. L.; Liu, H. Y.; Shen, Y. Y.; Zhang, J. R.; Zhu, J. *J. Anal. Chem.* **2011**, *83*, 661-665.

11. van Staden, J. F.; van Staden, R. I. S. *Talanta* **2012**, *102*, 34-43.

12. Anithaa, A. C.; Lavanya, N.; Asokan, K.; Sekar, C. *Electrochim. Acta* **2015**, *167*, 294-302.

13. Zhao, C.; Jiang, Z.; Cai, X.; Lin, L.; Lin, X.; Weng, S. *J. Electroanal. Chem.* **2015**, *748*, 16-22.

14. Alexander, C.; Bandyopadhyay, K. *Inorg. Chim. Acta* **2017**, *468*, 171-176.

15. Wang, J.; Yang, B.; Zhong, J.; Yan, B.; Zhang, K.; Zhai, C.; Shiraishi, Y.; Du, Y.; Yang, P. *J. Coll. Interface Sci.* **2017**, *497*, 172-180.

16. Guler, M.; Turkoglu, V.; Kivanc, M. R. *Electroanal.* **2017**, *29*, 2507-2515.

17. Guler, M.; Turkoglu, V.; Bulut, A.; Zahmakiran, M. *Electrochem. Acta* **2018**, *263*, 118-126.

18. Bisht, A.; Gangwar, B. P.; Anupriya, T.; Sharma, S. *J. Solid State Electrochem.* **2014**, *18*, 197-206.

19. Sun, C.; Li, H.; Chen, L. *Energy Environ. Sci.* **2012**, *5*, 8475-8505.

20. Liu, H. J.; Feng, Z. Y.; Huang, X. W.; Long, Z. Q.; Wang, M.; Xiao, Y. F.; Hou, Y. K. *J. Rare Earths* **2013**, *31*, 174-179.

21. Chen, L.; Si, Z. C.; Wu, X. D.; Weng, D.; Ran, R.; Yu, J. *J. Rare Earths* **2014**, *32*, 907-917.

22. Guler, M.; Turkoglu, V.; Basi, Z. *Electrochim. Acta* **2017**, *240*, 129-135.

23. Tan, L.; Zhou, K. G.; Zhang, Y. H.; Wang, H. X.; Wang, X. D.; Guo, Y. F.; Zhang, H.L. *Electrochem. Commun.* **2010**, *12*, 557-560.

24. Gan, T.; Sun, J.; Cao, S.; Gao, F.; Zhang, Y.; Yang, Y. *Electrochem. Acta* 2012, 74, 151-157.

25. Bard, A. J.; Faulkner, L. *R. Electrochemical Methods: Fundamentals and Applications*; John Wiley and Sons: Hoboken, NJ, USA, 2000.

26. Konopka, S. J.; McDuffie, B. *Anal. Chem.* **1970**, *42*, 1741-1746.

27. Laviron, E. *J. Electroanal. Chem. Interfacial Electrochem.* **1970**, *101*, 19-28.

28. Huang, J.; Liu, Y.; Hou, H.; You, T. *Biosens. Bioelectron.* **2008**, *24*, 632-637.

29. Aparna, T. K.; Sivasubramanian, R.; Dar, M. A. *J. Alloy Compd.* **2018**, *741*, 1130-1141.

30. Devnani, H.; Ansari, S.; Satsangee, S. P.; Jain R. *Mater. Today Chem.* **2017**, *4*, 17-25.

31. Zhu, Q.; Bao, J.; Huo, D.; Yang, M.; Wu, H.; Hou, C.; Zhao, Y.; Luo, X.; Fa, H. *J. Electroanal. Chem.* **2017**, *799*, 459-467.

32. Fazioa, E.; Spadaro, S.; Bonsignore, M.; Lavanya, N.; Sekar, C.; Leonardi, S. G.; Neri, G.; Neri, F. *J. Electroanal. Chem.* **2018**, *814*, 91-96.

33. Chu, K.; Wang, F.; Zhao, X. L.; Wang, X. W.; Tian, Y. *Mater. Sci. Eng. C* **2017**, *81*, 452-458.

34. Zhao, L.; Cai, Z.; Yao, Q.; Zhao, T.; Lin, H.; Xiao, Y.; Chen, X. *Sens. Act. B Chem.* **2017**, *252*, 1113-1119.

35. Cheng, M.; Zhang, X.; Wang, M.; Huang, H.; Ma, J. *J. Electroanal. Chem.* **2017**, *786*, 1-7.

36. Atta, N. F.; El-Kady, M. F.; Galal, A. *Anal. Biochem.* **2010**, *400*, 78-88.

37. Thiagarajan, S.; Yang, R. F.; Chen, S. -M. *Bioelectrochem.* **2009**, *75*, 163-169.

38. Yadav, S. K.; Rosy, Oyama, M.; Goyal, R. N. *J. Electrochem. Soc.* **2014**, *161*, H41-H46.

39. Wang, X.; Wu, M.; Tang, W.; Zhu, Y.; Wang, L.; Wang, Q.; He, P.; Fang, Y. *J. Electroanal. Chem.* **2013,** *695*, 10-16.

40. Palanisamy, S.; Ku, S.; Chen, S. M. *Microchim. Acta* **2013**, *180*, 1037-1042.

41. Guler, M.; Turkoglu, V.; Kivrak, A.; Karahan, F. *Mater. Sci. Eng. C* **2018**, *90*, 454-460.

42. Huang, J.; Liu, Y.; Hou, H.; You, T. *Biosens. Bioelectron.* **2008**, *24*, 632-637.

43. Bulut, A.; Yurderi, M.; Karatas, Y.; Zahmakiran, M.; Kivrak, H.; Gulcan, M.; Kaya, M. *Appl. Catal. B: Environ.* **2015**, *164*, 324-333.